LAWRENCE
LIVERMORE
NATIONAL
LABORATORY

LLNL-JRNL-413589

Numerical Modelling of the Nonlinear ELM Cycle in Tokamaks

A. Wingen, T. E. Evans, C. J. Lasnier, K. H. Spatschek

June 4, 2009

Physical Review Letters

Disclaimer

Numerical modelling of the nonlinear ELM cycle in tokamaks

A. Wingen[1], T.E. Evans[2], C.J. Lasnier[3], and K.H. Spatschek[1]
[1] *Institut für Theoretische Physik, Heinrich-Heine-Universität Düsseldorf, D–40225 Düsseldorf, Germany*
[2] *General Atomics, San Diego, California, 92186-5608, USA*
[3] *Lawrence Livermore National Laboratory, Livermore, California 94550, USA*
(Dated: May 29, 2009; printed May 29, 2009)

A numerical model of the nonlinear evolution of edge localized modes (ELMs) in tokmaks is presented. In the model discussed here it is assumed that thermoelectric currents flow in short connection length flux tubes, initially established by error fields or other non-axisymmetric magnetic perturbations. Magnetic perturbations resulting from the currents are incorporated into the magnetic topology. The predictions are compared to measurements at the DIII-D tokamak. Excellent agreement between the calculated magnetic structures on the vessel wall and camera observations during an ELM cycle is shown. The ELM collapse process is discussed.

PACS numbers: 05.45.a,05.45.Pq,28.52.Av,52.35.Py,52.55.s,52.55.Fa,52.55.Rk,52.55.Wq

Edge localized modes (ELMs) [1] are common phenomena in stationary H-mode plasmas in the current generation of tokamaks. Control and mitigation of high heat loads expelled by ELMs is a key topic for the next generation fusion devices like ITER. The type-I ELMing H-mode is the standard operational scenario for ITER [2]. Extrapolating the power expelled by ELMs in ITER implies that plasma facing wall materials will suffer from fast erosion or melting [3]. ELM-like processes are also of importance in other fields such as solar flare astrophysics. Both solar flares and ELMs involve magnetized plasma eruptions, however in different regimes of magnetized plasma physics, which sporadically eject field-aligned filamentary structures into the surrounding vacuum region [4].

Still there are significant gaps in our understanding of the ELM evolution beyond the initial linear phase. It is unknown how the nonlinear evolution scales with plasma geometry and operating conditions as well as why they are mitigated and suppressed by certain resonant magnetic perturbations (RMPs) within special parameter conditions. The use of edge stochastization has been shown to significantly influence ELM dynamics [5] and plasma-wall interaction. Because of their vital impacts, perturbation coils have been installed in various tokamaks, like Tore Supra, TEXTOR, DIII-D and JET. In DIII-D RMPs have successfully been used in ELM suppression [6]. Also in JET type-I ELM mitigation was recently successfully achieved by RMP [7]. Motivated by these results, a flexible set of RMP coils was added to the ITER design [8, 9] in the recent design review process. Thus, there is an urgent need for a model that can be tested with experimental data from existing devices. Such a model is presented here and verified against measurements in the DIII-D tokamak.

Peeling-ballooning theory predicts that a Type-I ELM cycle is initiated when an edge ideal MHD mode is destabilized as the pedestal pressure gradient exceeds the linear marginal stability limit of the mode [10]. This produces an initial pulse of heat and particles. As described in Ref. [11] this pulse is conducted towards the target plates and arrives at the outer target plate well before it arrives at the inner target plate. Due to the different arrival times, the heat pulse instantaneously increases the electron temperature T_e on the outer target relative to the inner target plate. Thus, a thermoelectric current is driven between the targets, flowing from the outer to the inner target plate [12]. Since this current can cause a substantial change in the edge topology of the plasma, it is important to understand the path that it follows.

In recent works, measurements of fluctuations in the poloidal magnetic field during ELMs in DIII-D were reproduced numerically by running currents in the scrape-off layer [13]. Also, the influence of RMPs on the magnetic topology in DIII-D has been analyzed in great detail. Separatrix splitting into stable and unstable manifolds and connection of internal resonant islands to the targets has been investigated [14]. Also the formation of short connection length flux tubes has been shown [15]. The latter connect the target plates through the plasma edge within the perturbed separatrix boundary. Within the flux tubes a coherent non-stochastic structure is maintained while being surrounded by stochastic field lines. These flux tubes are the perfect candidates for conducting the thermoelectric current since they represent a short and coherent path through the plasma.

Figure 1 shows a connection length simulation of the lower target area poloidal cross-section in DIII-D. The color code represents the connection length of the field lines, which is the field line length inside the vessel between the two target plates. The simulation is constrained to match experimental data from shot# 133908 at 2000 ms. These data are used as examples for a typical ELMing H-mode shot with error fields and error field correction coils active (the I-coil is used for error field correction here). In the following, this shot is referred to as the reference case. As can be seen, the magnetic topology is only slightly perturbed by the combined error

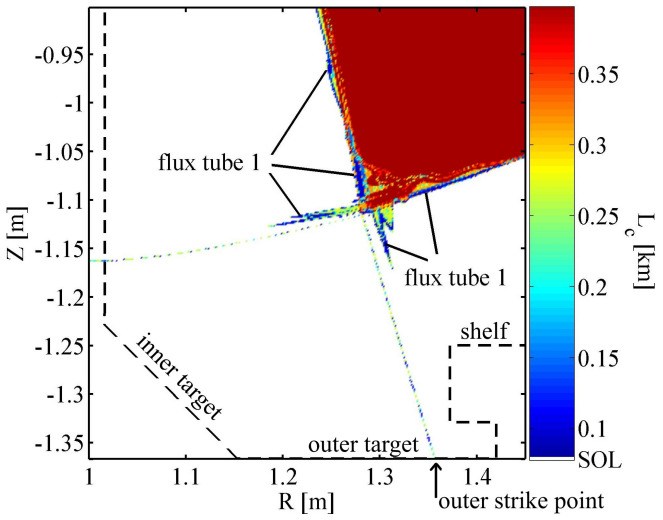

FIG. 1: Connection length plot of the lower target area in DIII-D of shot# 133908 at 2000 ms. The dashed line shows the wall of the vacuum vessel. The inner and outer targets are named as well as the shelf. The position of the outer strike point is marked by the black arrow. The poloidal cross-section is at the toroidal angle $\phi = 0°$. The white area gives the scrape-off layer (SOL), the area outside of the separatrix plasma boundary.

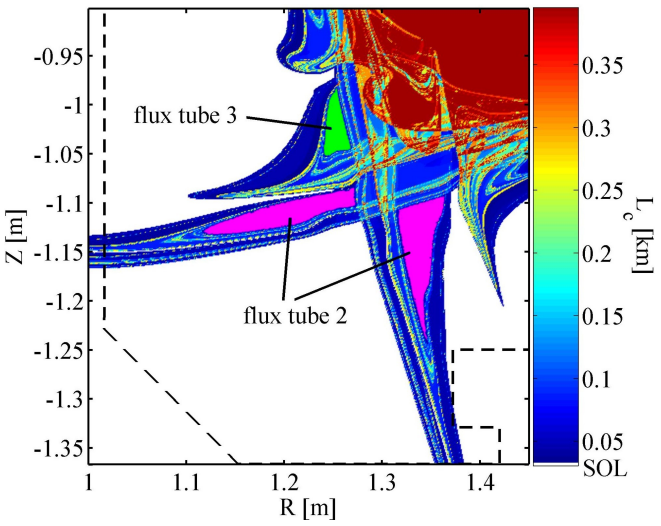

FIG. 2: Poloidal cross section of the bifurcated structure produced when a 300 A current filament is driven in tube 1, shown in Fig. 1. The structure of flux tube 2 is shown by the magenta areas and flux tube 3 is shown by the green area. Their connection length is about 50 m. Note that the green and magenta colors are intended to highlight these flux tubes, and do not correspond to the color scale at the right.

and I-coil fields. One flux tube appears, which intersects several times with the poloidal cross-section, as shown by the small blue areas in Fig. 1. This flux tube has a connection length of about 100 m or two poloidal turns. As discussed in Ref. [15], the flux tube is created by the intersection of the stable and unstable separatrix manifolds. In the following it will be referred to as tube 1. Its area is approximately 2.1 cm^2 which scales as 1/B since the toroidal flux ($B_T \cdot dA$) is preserved due to the symplectic nature of the Hamiltonian system.

The model simulated here consists of two steps and is based on a new ELM model proposed in Ref. [11]. In the first step an initial current of 300 A is assumed flowing through tube 1. This assumption will be verified later. The magnetic field perturbation of this current modifies the topology of the plasma edge severely. Three main new effects appear. First a connection to the upper target plates is established. The former lower single null configuration turns into a double null configuration. The second effect is that a new type of flux tube appears. The new flux tubes are indirect evidence for the additional connection to the upper targets, since the latter is not explicitly shown in this letter. Each of the new flux tubes still connects the two lower targets with each other, but its area is very large, e.g. 22.5 cm^2, compared to tube 1. Also, the connection length is only one poloidal turn or about 50 m, which is half the length of tube 1. The area of these tubes formerly belonged to the scrape-off layer.

The modified topology is shown in Fig. 2. As can be seen, several new flux tubes appeared: one poloidal turn tubes as well as longer ones similar to tube 1 (also tiny 1 1/2 poloidal turn tubes, connecting the lower to the upper targets). The third effect is that a bifurcation is caused by the current perturbation. In the reference case there is only one flux tube with a certain toroidal phase. In the modified topology every flux tube has a counterpart whose phase is shifted by 180° toroidally. The flux tubes can be ordered in pairs while each pair forms a double helical like structure.

In the second step we assume that a thermoelectric current flows through the newly created much shorter, one poloidal turn flux tubes. Let us pick the two largest ones, marked in Fig. 2 as flux tube 2 (magenta) and flux tube 3(green). Thereby, tube 3 is the 180° shifted counterpart of tube 2. Note that all one poloidal turn flux tubes have the same helical structure as either tube 2 or tube 3 and therefore produce similar $n = 2$ perturbations.

To estimate the current flowing through tube 2 and 3 we assume the current density to be constant and scale the total current by the area of the flux tube. According to current measurements presented in [11], the peak current flowing through e.g. the tile at $\phi = 265°$ is about 150 A (the measuring tiles are shown in Fig. 3 as dashed lines). Using the ratio of the area on the tile covered by tube 2 and 3 and the total area of both tubes on the target, we can estimate the total current to be 4.6 kA. According to the individual areas of tube 2 and 3 in the poloidal cross-section, Fig. 2, we conclude that tube 2 carries a current of 2.8 kA and tube 3 carries a current of 1.8 kA. Using the same area scaling, we get a current of about 272 A in tube 1, which confirms our initial assumption.

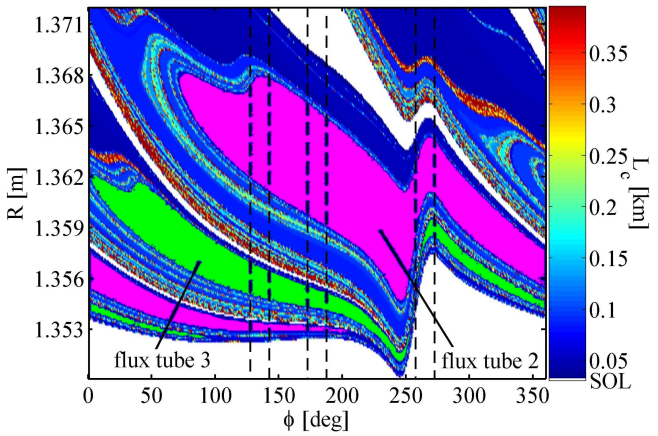

FIG. 3: Connection length footprint on the outer target plate with the additional perturbation of the 300 A current filament in tube 1. The dashed lines show the position and extent of the current measuring tiles. Note that the outer target has a vertical step up to the shelf at $R = 1.372$ m (see Fig. 1), which is the top boundary of Fig. 3. The toroidal angle is given in the left-handed machine related coordinate system. Flux tube 2 and 3 are shown similar to Fig. 2.

Comparing with experiments we note that during shots in DIII-D a camera takes pictures of the shelf, located above the outer target, which starts at the major radius $R = 1.372$ m at $Z = -1.250$ m. During an ELM event stripes appear on the shelf, as can be seen in Fig. 4(a). The lowest very bright stripe in the image is created by the outer strike point and marks the beginning of the shelf as well. Different tiles are clearly visible in the light of the discharge as well as an upward viewing vertical port located at $R = 1.486$ m, $\phi = 60°$ in the vessel near the right-hand edge of the of the shelf shown in Fig. 1. At the very beginning of the shelf a faint stripe is visible, which almost merges with the bright light from the strike point, located at $Z = -1.366$ m on the divertor target plate as seen in Fig. 1. Further out radially on the shelf three stripes are clearly visible, one right below the port, one very bright one hitting the lower part of the port and a smaller one hitting to top of the port. These are typical stripe structures that appear on the shelf during ELMs.

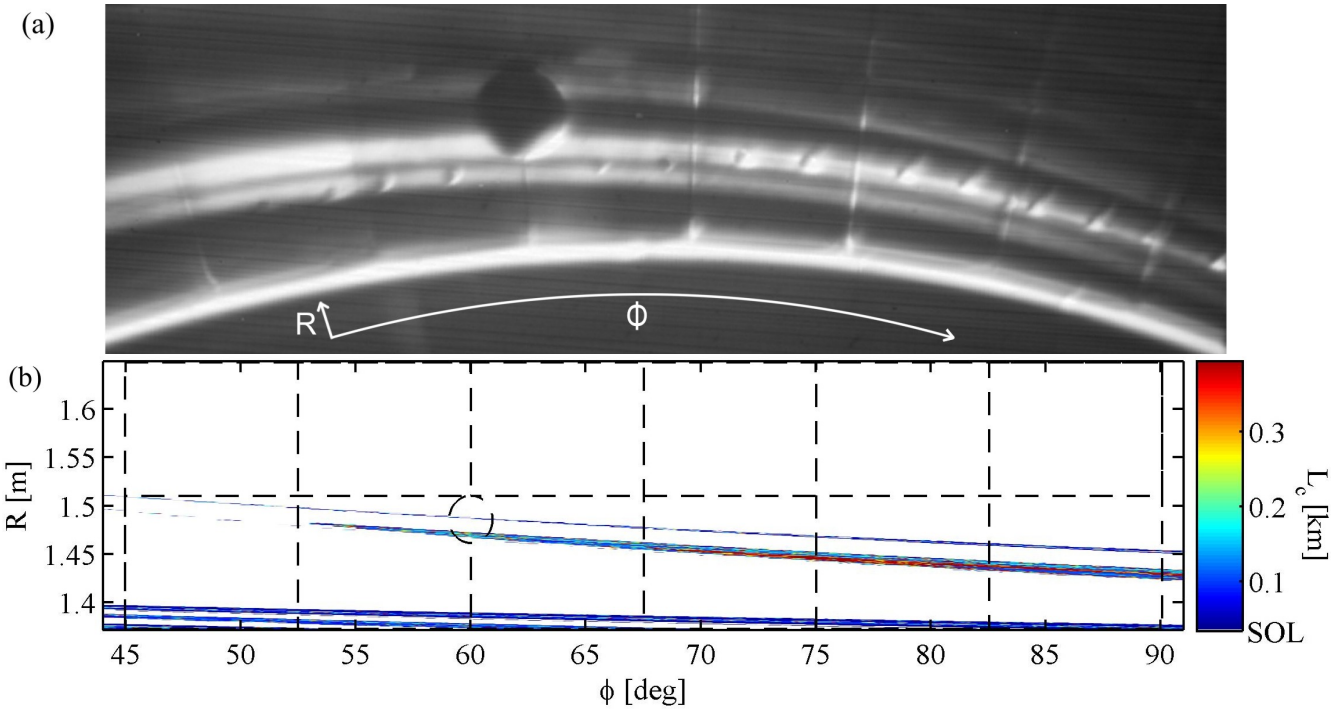

FIG. 4: (a) Infrared camera observation of an ELM event. Shot# 133908 close to 2000 ms. The camera view shows the shelf, starting at $R = 1.372$ m and $Z = -1.250$ m (below the equatorial plane of the tokamak), around the port at $\phi = 60°$, visible as a dark circle. As seen in Fig. 1, the outer target plate is located at $Z = -1.366$ m or 0.116 m below the top of the shelf.
(b) Connection length plot of the same section on the shelf as shown in (a). The dashed lines indicate the different tiles and the port, as they are visible in the camera picture. Currents of 300 A in tube 1, 2.8 kA in tube 2 and 1.8 kA in tube 3 are used in the numerical model to produce the striped footprint pattern on the top of the shelf seen in (b).

Figure 4(b) shows a connection length simulation of the same region on the shelf as in Fig. 4(a). The various tiles as well as the port are indicated by dashed lines. Note that the numerical predictions are depicted in cylindrical

coordinates while the camera observations in Fig 4(a) are shown in Cartesian coordinates. This different display explains the missing curvature in Fig. 4(b). The numerical model, which includes the thermoelectric currents in the flux tubes, clearly shows nearly the same ELM stripe structure as can be seen in the camera image. There are small stripes at the very edge of the shelf, which is the bottom boundary in the figure. A large stripe with high connection length hits the lower part of the port and a small stripe hits the upper part. The major radius of the stripes increases with decreasing toroidal angle. The same trend is clearly visible in the camera image. So, by taking into account the thermoelectric currents in short connection length flux tubes, ELM stripe structures can be reproduced numerically with good accuracy.

The ELM collapses a few ms after its initiation. Here, experimental observations suggest that a relatively complex process may be involved in disrupting the thermoelectric current in the flux tubes. There are several possibilities for understanding this phenomenon. First, as already discussed in Ref. [11], the heat stored in the pedestal, which supports the temperature gradient between the targets, is depleted during the ELM. Once the temperature gradient equilibrates, the thermoelectric current collapses. Another possibility can be seen from the flux tube itself. Once the high currents start flowing inside the one poloidal turn flux tubes, the magnetic topology is changed. The flux tubes themselves could be destroyed, resulting in a disruption of the current and a return to the reference state.

The model presented here has certain limitations. First, it is not completely self-consistent since an iterative two step description was used. Therefore, it cannot be used to simulate the actual time evolution of the ELM. Also, only single current filaments were used here instead of a more realistic current distribution over the whole flux tube area. On the other hand, the magnetic field perturbation of the current filaments is precalculated on a dense grid covering part of the area contained within the flux tube and then interpolated between grid points during runtime. By this, the B-field singularity at the position of an infinitesimally small current filament is prevented.

Despite these limitations in this Letter it is shown for the first time that typical ELM stripe structures can be correctly modelled when the thermoelectric currents are incorporated. The stripes in the connection length plot, Fig. 4(b), appear at the same positions, radially and toroidally, and with the same radial outward trend as in the camera observation in the discharge. The currents used in the model are scaled in agreement with current measurements during ELM events. Furthermore, the simulation shows, indirectly through the formation of the new flux tubes, that a connection of the plasma with the upper targets is established during the process. The simulations presented here provide a proof-of-principle confirmation of the model proposed in Ref. [11] stating that perturbations of the plasma edge which create the filamentary structures observed during an ELM cycle are driven by thermoelectric currents flowing through short connection length flux tubes. Furthermore, it has been shown that the seed flux tubes needed to initiate this process are generated by small non-axisymmetric magnetic perturbations such as field errors which are always present in magnetic confinement devices like tokamaks. The sensitivity of the results on the initial topology will be studied in the future. Such a sensitivity could provide a mechanism for variations in the ELM-to-ELM footprint pattern.

In future work the model will be improved with respect to the limitations mentioned above. Especially the effect of a broader current distribution within the flux tubes will be investigated. Preliminary modelling of broader current distributions show that the main features of the simulation discussed above remain while an even more complex substructure may be created. The effect of other types of RMPs on the ELM structures will be studied in the future with the main goal to predict and understand ELM suppression numerically.

Discussions with R. A. Moyer, O. Schmitz and M. Jakubowski are gratefully acknowledged. This work was supported by the US Department of Energy under Grant Nos. DE-FC02-04ER54698, DE-AC52-07NA27344 and DE-FG02-05ER54809, as well as the DFG under project SP229/1-1.

Prepared by LLNL under Contract DE-AC52-07NA27344.

[1] H. Zohm, Plasma Phys. Contr. Fusion **38**, 1213 (1996).
[2] M. Shimada, et al., Nucl. Fusion **47**, S1 (2007).
[3] A. Loarte, et al., Plasma Phys. Contr. Fusion **45**, 1549 (2003).
[4] W. Fundamenski, et al., Plasma Phys. Contr. Fusion **49**, R43 (2007).
[5] T. E. Evans, et al., Nature Physics **2**, 419 (2006).
[6] T. E. Evans, et al., Phys. Rev. Lett. **92**, 235003 (2004).
[7] Y. Liang, et al., Phys. Rev. Lett. **98**, 265004 (2007).
[8] M. Bécoulet, et al., Nucl. Fusion **48**, 024003 (2008).
[9] M. J. Schaffer, et al., Nucl. Fusion **48**, 024004 (2008).
[10] H. R. Wilson, et al., Plasma Phys. Contr. Fusion **48**, A71 (2006).
[11] T. E. Evans, et al., J. Nucl. Mater. **390-391**, 789 (2009).
[12] G. M. Staebler and F. L. Hinton, Nucl. Fusion **29**, 1820 (1989).
[13] H. Takahashi, E. D. Fredrickson, and M. J. Schaffer, Phys. Rev. Lett. **100**, 205001 (2008).
[14] A. Wingen, T. E. Evans, and K. H. Spatschek, Phys. Plasmas **16**, 042504 (2009).
[15] A. Wingen, T. E. Evans, and K. H. Spatschek, Nucl. Fusion **49**, 055027 (2009).